Journal of Hazardous Materials 189 (2011) 167–172

Contents lists available at ScienceDirect

Journal of Hazardous Materials

journal homepage: www.elsevier.com/locate/jhazmat

Experimental design of application of nanoscale iron–nickel under sonication and static magnetic field for mixed waste remediation

Ritu D. Ambashta[a,b,*], Mika Sillanpää[a,c]

[a] University of Eastern Finland, Laboratory of Applied Environmental Chemistry, Patteristonkatu 1, FI-50100 Mikkeli, Finland
[b] Backend Technology Development Division, Bhabha Atomic Research Centre, Mumbai 400085, India
[c] Faculty of Technology, Lappeenranta University of Technology, Patteristonkatu 1, FI-50100 Mikkeli, Finland

ARTICLE INFO

Article history:
Received 19 August 2010
Received in revised form 6 December 2010
Accepted 7 February 2011
Available online 15 February 2011

Keywords:
Organics degradation
Nanoscale iron–nickel
Sonication
Magnetic field
Radioactive

ABSTRACT

In this paper, the degradation of simulated mixed organics commonly found in nuclear waste streams was studied under a combined influence of sonication and magnetic field. Nanoscale bimetallic iron–nickel was used as source of Fenton reaction. The data were fitted to obey second order kinetics. The extent of degradation followed the trend: TBP-EDTA-citric acid greater than TBP-EDTA, greater than TBP alone. The influence of the three variables that govern degradation behaviour viz. sonication energy, magnetic field and time were evaluated with response surface methodology. The model could predict the ratio of total organic carbon content to a maximum error of only ~6%.

1. Introduction

The management of mixed wastes, which contain both radionuclides and toxic chemicals, poses a major challenge to scientists and engineers charged with the daunting task of stabilising and disposing them. The origin of mixed wastes can be quite varied. Some have been generated during reprocessing of spent nuclear fuel, while others are generated in commercial nuclear operations [1–5]. Organic substances present in radioactive wastes make the waste management upon storage and disposal more difficult. These compounds may be responsible for a chemical explosion similar to that happened in Kyshtym (Russia) in 1957; as a result of which a large area in the south Ural Mountains was radioactively contaminated. Moreover, organic substances increase the yield of gases (among them are explosive hydrogen and methane) upon radiolysis by radiation from radionuclides present in the waste [6,7]. In some laboratories, these wastes have been stabilized in cementitious grouts but it has been observed that in due course there is enhancement of the environmental mobility of certain radionuclides leached from these wasteforms. The stronger the chelant complex (between organic and radionuclide), the higher is the probability of leaching of compound [1,8–11]. Chemical precipitation and ion-exchange are common treatment methods for separation of radionuclides from aqueous waste streams. In the presence of organic chelants the radioactive cations form complexes which cannot be removed by the conventional techniques and there is poor decontamination factor obtained [12]. It is therefore important to destroy the organic impurities in the wastes.

Irradiation techniques are non-incinerative methods used to destroy the organic constituents of mixed wastes [13,14]. Although incineration can accomplish these objectives, it poses some formidable problems, including release of acid gases (NOx and SOx), formation of chlorinated dibenzodioxins and dibenzofurans, and release of radioactive fly-ash, which can be hard to control [15]. Other techniques for organic pollutants destruction include chemical oxidation/reduction technologies, electrochemical oxidation/reduction, biological processes, photolytic degradation, degradation using zerovalent iron and degradation based on Fenton reaction [16–19].

The commonly found organics that interfere with chemical precipitation processes in mixed wastes from nuclear program origin include tributyl phosphate (TBP), ethylene diamine tetraacetic acid (EDTA), citric acid (CA) and their irradiation degraded products. Dodecane (DD) is invariably accompanied as a diluent with TBP. In the present study, a simulated waste of TBP, DD, EDTA and CA with ions of cerium, ruthenium, strontium and cesium was prepared.

The corrosion reaction using bimetallic or zero-valent iron has been exploited for the degradation of several organics [20–24]. Nickel aides in enhancing the corrosion of iron and extensive

* Corresponding author at: Backend Technology Development Division, Bhabha Atomic Research Centre, Mumbai 400085, India. Fax: +358 153556363.
E-mail addresses: aritu@barc.gov.in (R.D. Ambashta), Mika.Sillanpaa@uef.fi (M. Sillanpää).

0304-3894/$ – see front matter © 2011 Elsevier B.V. All rights reserved.
doi:10.1016/j.jhazmat.2011.02.021

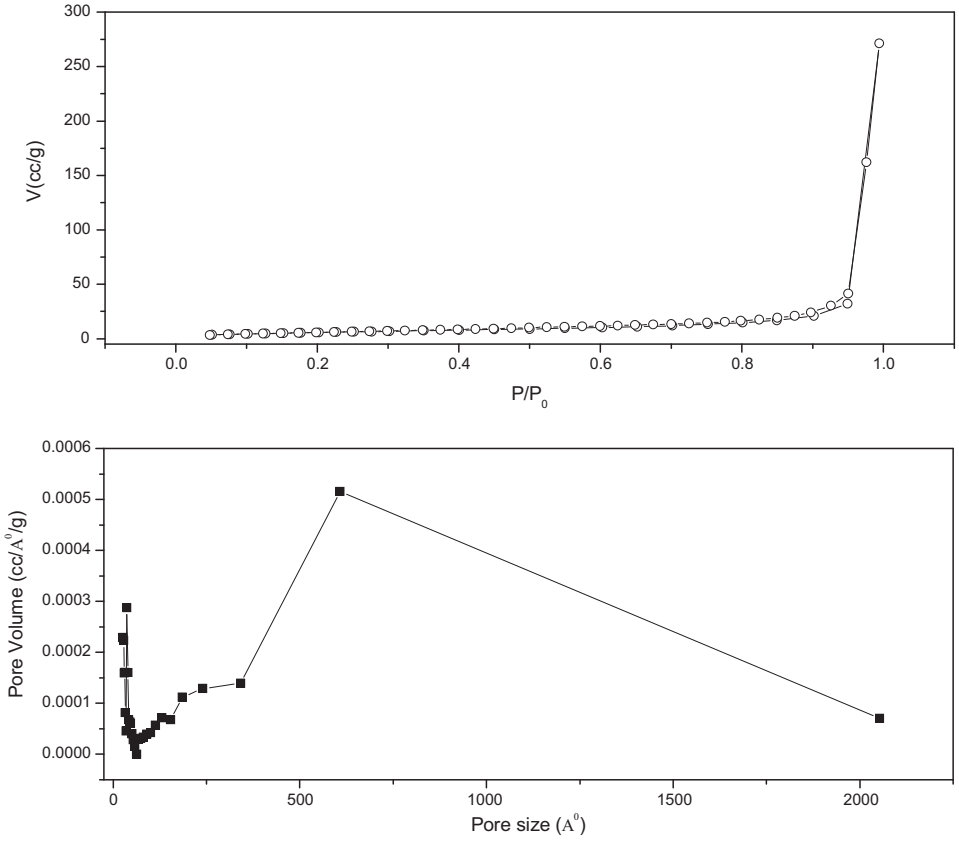

Fig. 1. The nitrogen adsorption–desorption isothermal curves of iron–nickel powders with the pore size distribution.

studies have been reported for iron–nickel for the degradation of organics [25–30]. The present paper also gives an experience on degradation of organics using nanoscale iron–nickel. Magnetically assisted chemical processing has been demonstrated for several applications in separation sciences, synthesis methods and catalytic methods [31–34]. Iron has an intrinsic magnetic moment. It has been observed that under the influence of magnetic field the zero-valent iron reactivity reduces due to agglomeration and therefore purpose of small size reactivity is lost [35]. The method of sonication has been applied in the degradation of organic compounds at different ultrasound frequencies [36–39]. It is a good dispersion source as well. Using nanopowder of iron–nickel a combination of sonication energy and magnetism has been exploited for the first time for the degradation of organics in mixed wastes. An experimental design of reactions was also evaluated for parameters of time, sonication energy and magnetic field respectively using surface response methodology.

2. Experiment

2.1. Materials and reagents

Nanopowders of iron–nickel [FE-NI-017-NP.100 N] were received from M/s American Elements. TBP, DD, EDTA, CA and nitric acid of AR grade were used in the experiments. Inductively coupled plasma (ICP) standard solutions of Ce, Ru, Cs and Sr were used in the experiments for simulating radionuclides. Increasing the organic component, three solutions namely A, B and C were prepared.

Solution A: 300 mg/L TBP (30% by volume in DD) was prepared in pH 4 solution of nitric acid containing 8 mg/L Ce, 8 mg/L Ru, 8 mg/L Cs and 0.8 mg/L Sr.

Solution B: A mixture of 300 mg/L TBP (30% by volume in DD) and 300 mg/L EDTA was prepared in pH 4 solution of nitric acid containing 8 mg/L Ce, 8 mg/L Ru, 8 mg/L Cs and 0.8 mg/L Sr.

Solution C: A mixture of 300 mg/L TBP (30% by volume in DD), 300 mg/L EDTA and 300 mg/L CA was prepared in pH 4 solution of nitric acid containing 8 mg/L Ce, 8 mg/L Ru, 8 mg/L Cs and 0.8 mg/L Sr.

2.2. Catalytic experiments for mixed waste remediation

DC powered electromagnet procured from M/s SVS Lab Inc was used in the experiments. The samples of iron–nickel were dispersed under sonication using 2510 Branson Sonicator, in different solutions of A, B and C. All reactions were carried out in a (7.5 mm ID × 250 mm H) flat bottom tube under a magnetic field of 0.8 T for different time durations.

2.3. Catalytic experiments for experiment design

The sonicator was changed to Hielscher Ultrasonics GmbH UPS4 model (working frequency 24 kHz, maximum amplitude 210 μm, maximum acoustic power density 460 W/cm^2) with a 3 mm diameter probe for variable sonication energy input for the reaction. The same DC powered electromagnet was used for generating a variation in background magnetic field between 0.1 and 0.8 T.

2.4. Characterization of materials

PANalytical X'Pert Pro MPD-model X-ray diffraction (XRD) was used to investigate the crystalline nature of the powders. Hitachi S-4800 Ultra-High Resolution Scanning Electron Microscope (SEM) was used to investigate the morphology of powder. The total organic carbon (TOC) content analysis was carried out

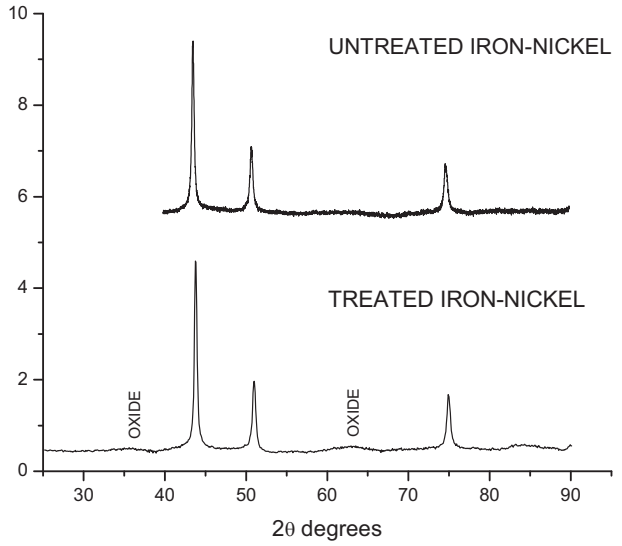

Fig. 2. XRD pattern of nanopowder of iron and nickel before treatment and after treatment of sonication under induced field of 0.3 T for 60 min.

using TOC-VCPH Shimadzu Analyzer. The standard deviation using TOC standard was <4%. Surface area, particle size and pore diameter were evaluated using Autosorb 1, Quanta Chrome Instruments. The elements Ce, Ru and Sr in the solution were analysed using Thermo Electron Corporation iCAP 6000 Series inductively coupled plasma-optical emission spectrometry (ICP-OES). The element Cs was analysed using inductively coupled plasma-mass spectrometry (ICP-MS).

3. Results and discussion

3.1. Powder characterization

The BET surface area and pore structure of samples were determined from nitrogen isothermal analysis as shown in Fig. 1. Using multipoint BET, BJH cumulative desorption and DH cumulative desorption methods, the average surface area of iron–nickel was evaluated as 27 m^2/g. The average pore diameter was 753 Å for iron–nickel and the total pore volume was 0.42 cm^3/g.

Maintaining the solution A (300 mg/L TBP in DD, 30% by volume in pH 4 nitric acid) to powder ratio at 1000:1 (volume [mL] by weight [g]), the samples were sonicated under induced magnetic field of 0.8 T for an hour. The comparison of XRD patterns and morphology of the samples sonicated for an hour under magnetic field of 0.8 T is shown in Fig. 2. The XRD pattern of untreated samples showed the presence of hexagonal close-packed iron–nickel (hcp FeNi). The XRD lines matched with the X-ray powder diffraction file number PDF 023-0297. Sonication under the influence of magnetic field formed additional phases which are a combination of inverse spinel nickel ferrite and other iron/nickel oxides.

The SEM images of the treated and untreated powder samples are shown in Fig. 3. The images suggested that after treatment, the spherical shape of the powders transformed to rod shape. Sonication aides in shredding of the particles to smaller diameter particles while the application of magnetic field aligns the particles in direction of field. The observation suggests that sonication aides in enhancing reactivity of powder while magnetism slows reactivity.

3.2. Mixed waste remediation

The samples of iron–nickel were dispersed under sonication in different solutions of A, B and C under a magnetic field of 0.8 T for different time durations. The solutions of 60 min reaction were analysed for the element content using ICP. The percent extraction data is summarized in Table 1. The data suggest that each element was sorbed to a certain extent on the mixed oxide formed as a result of oxidation of metal content and owing to large surface area of the powder. This suggests that dual role of nanopowders as organic destructant and ion sorbent is possible using the present mode of application. The plot of ratio of final to initial total organic carbon versus time is shown in Fig. 4. The 300 mg/L TBP in DD (volume proportion 30%) showed reduction in organic carbon content by 25%. The addition of 300 mg/L EDTA (solution B) reduced the organic carbon content by 30% while further addition of 300 mg/L citric acid (solution C) reduced carbon content by 40%. The data were fitted to second order equation [40]. The rate of reactions in terms of TOC data was evaluated as 0.1551 mg/L/min for TBP-DD, 0.2411 mg/L/min for TBP-DD-EDTA and 3.516 mg/L/min for TBP-DD-EDTA-CA.

The presence of carboxylic acid aided in enhancing the rate of iron nickel corrosion which led to enhanced extent degradation of organics. The reason for the same can be understood from the following. EDTA and CA form strong complexes with transition series

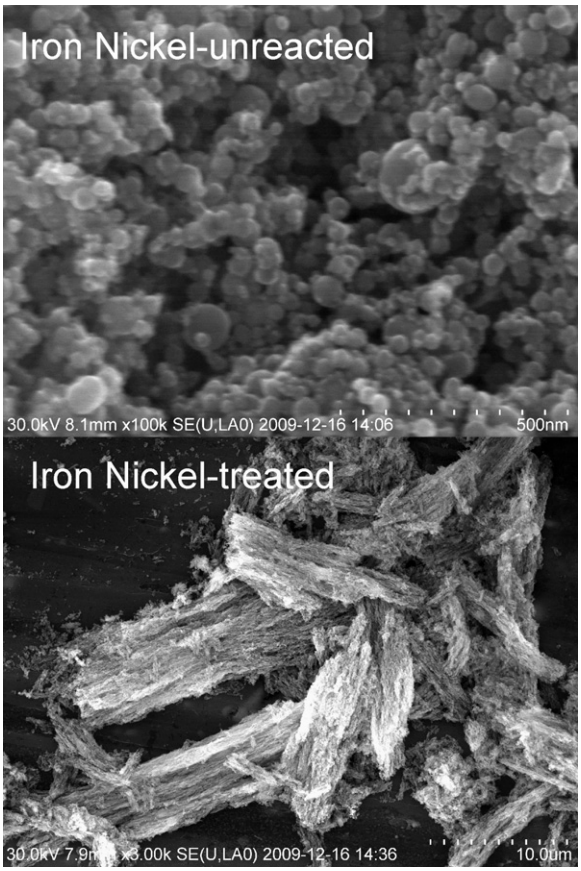

Fig. 3. SEM image of nanopowder of iron and nickel before treatment and after treatment of sonication under induced field of 0.3 T for 60 min.

Table 1
The percent extraction values of elements added to simulate radioactive constituents in mixed wastes.

Sample	Ce	Ru	Sr	Cs
TBP-dodecane	3.3	1.6	3.3	1.4
TBP-dodecane-EDTA	8.0	10.6	4.6	1.9
TBP-dodecane-EDTA-CA	13.7	11.9	4.6	1.9

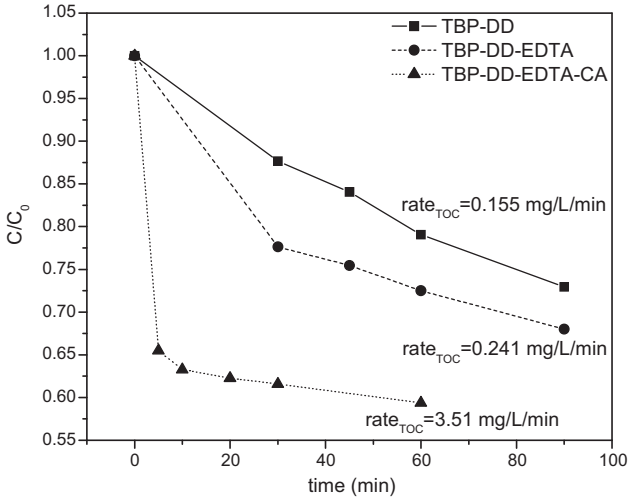

Fig. 4. Ratio of final to initial organic carbon content for solution A, B and C versus time. Rate in terms of TOC is expressed in inset.

elements. Iron–nickel degrades TBP according to the mechanism,

$$M^0 + O_2 + 2H^+ \rightarrow M^{2+} + H_2O_2 \quad (1)$$

$$H_2O_2 \rightarrow H_2O + 1/2O_2 \quad (2)$$

$$(C_4H_9O)_3PO + 18O_2 \rightarrow 12CO_2 + 3H^+ + PO_4{}^{3-} + 12H_2O \quad (3)$$

Alternatively,

$$M^{2+} + H_2O_2 \rightarrow MOH^{2+} + OH^\bullet \quad (4)$$

$$(C_4H_9O)_3PO + OH^\bullet \rightarrow (C_4H_9O)_2(C_4H_8O)PO + H_2O \quad (5)$$

EDTA interaction with metal powder is according to the mechanism,

$$M^0 + EDTA + H_2O \rightarrow [M^{II}(EDTA)(H_2O)]^{2-} \quad (6)$$

$$[M^{II}(EDTA)(H_2O)]^{2-} + O_2 \rightarrow [M^{II}(EDTA)O_2]^{2-} + H_2O \quad (7)$$

$$[M^{II}(EDTA)O_2]^{2-} \rightarrow [M^{II}(EDTA)O_2{}^-]^{2-} \quad (8)$$

$$[M^{II}(EDTA)(H_2O)]^{2-} + [M^{III}(EDTA)(O_2{}^-)]^{2-} \rightarrow [(EDTA)M^{III}(O_2{}^{2-})M^{III}(EDTA)]^{4-} + H_2O \quad (9)$$

$$[(EDTA)M^{III}(O_2{}^{2-})M^{III}(EDTA)]^{4-} \rightarrow 2[M^{III}(EDTA)H_2O]^- + H_2O_2 \quad (10)$$

$$M^{II}EDTA + H_2O_2 \rightarrow M^{III}EDTA + OH^- + OH^\bullet \quad (11)$$

Similar interaction with CA is expected. The mechanism suggests that carboxylic acid aides in production of more H_2O_2, the primary constituent responsible for degradation of the organics. We conclude that as we move from solution A to C, the extent of degradation of organics increases in accordance with above mechanism.

The degradation behaviour of TBP has been extensively studied. Using UV fluence of 1000 mJ/cm^2, TBP was degraded with a rate of $k_{OH} \sim 6.4 \times 10^9$ M^{-1} s^{-1} [41]. Biomass degraded TBP in the presence of uranium at the rate of 37 μmol h^{-1} mL^{-1} in terms of the biomass content [42]. Photosynthetic bacteria degraded 2 mM of TBP at the rate of 0.48 mM h^{-1} of bacterial content [43]. The degradation of EDTA and CA was carried out using irradiation such as gamma energy. The first order rate of ~1 h^{-1} was followed for the same [14,17]. Biodegradation of EDTA followed at the rate of 15 μmol h^{-1} of biomass content [44]. In Fenton systems or in applications of zerovalent iron, complexing agents like EDTA and citric acid were used to activate the dissolved oxygen and assist in hydrogen peroxide production [45–49].

The UV-H_2O_2 method of degradation required dilution of wastes. This added to the total volume which is not desireable from radiotoxicity volumes handling point of view. Application of biomass increased sludge content which is not desireable since it needs separate treatment. In the present experimental study, hydrogen peroxide was in situ generated; therefore, there was no effective increase in volume of solution. The magnetic material not only degraded the organic compound but also accommodated radionuclides to a certain extent and helped in improving the effective decontamination of radionuclides.

3.3. Experimental design construction

The experimental design construction attempted was based on three variables: sonication energy, applied magnetic field and time. The other factors catalyst concentration, organic concentration, pH of reaction were maintained as constant factors and therefore not included in the design construction. Response surface methodology is based on the hypothesis that the responses can be approximated, within the range of the data, by a low order polynomial model. The responses were assumed to be a function of the coded variables X_i' (time, sonication energy and magnetic field) and the postulated model was a special cubic polynomial in the canonical form [50–57].

$$Y = \sum_{i=1}^{3} \beta X + \sum_{1 \le i < j}^{3} \beta_{ij} X_i' X_j' + \sum_{1 \le i < j < k}^{3} \beta_{ijk} X_i' X_j' X_k' + \varepsilon \quad (12)$$

where Y = experimental response (ratio of TOC) and ε = random error. The unmixed squared and cubic terms did not yield a good model and therefore were ignored. In this second model, the first-order coefficients (β_i) predict the response Y from the pure components. The second-order (β_{ij}) and third order terms (β_{ijk}) reveal interactions: positive interaction coefficients indicate synergism, i.e. the two components together work better than either one alone. Negative interaction coefficients mean antagonism between components, i.e. the two components work against each other to make the response variable less expressed. The model can be written in matrix notation as

$$Y = XB + e \quad (13)$$

where Y is the $(n \times 1)$ vector of responses, X is the $(n \times p)$ matrix of model terms, B is the $(p \times 1)$ vector of unknown coefficients and e is the $(n \times 1)$ vector of errors with zero means and variance $\sigma^2 I$, σ^2 being the experimental error variance and I the $(n \times n)$ identity matrix. B, the least squares estimate of B is defined as

$$\hat{B} = (X'X)^{-1}X'Y \quad (14)$$

It can be easily shown that the variance–covariance matrix for $\hat{B}$ checks

$$\mathrm{Var}(\hat{B}) = (X'X)^{-1}\sigma^2 \quad (15)$$

Calculations were performed using Octave version 3.2.4 (http://www.octave.org).

The time was varied from 5 min to 60 min, the sonication energy was varied between 20 and 100% and the magnetic field was varied from 0.1 T to 0.8 T. After normalising the variables, a ternary plot (refer Fig. 5) of sonication energy, magnetic field and time were obtained. Taking data of extreme vertices of seven experiments in the ternary plot, the polyhedron was constructed to depict the response surface under evaluation. This response surface signifies

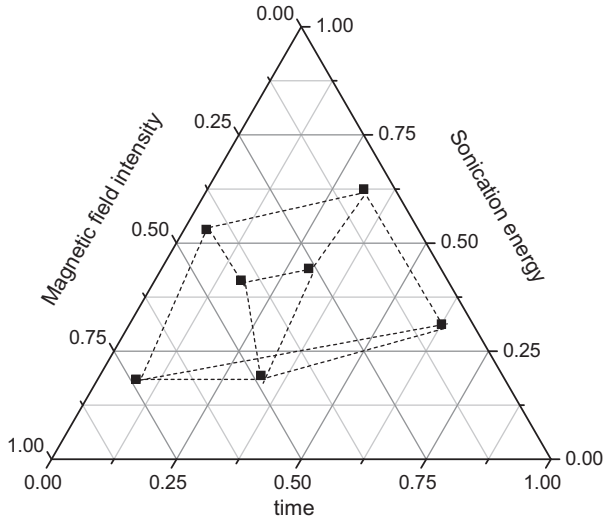

Fig. 5. Ternary plot of time, sonication energy and magnetic field depicting domain of coordinates included in the model. The coordinates were joined to form of polyhedron whose response surface was evaluated.

Table 2
The experimental and calculated values of ratio of final to initial total organic carbon content of coordinates included in the model with variance and variance of coefficient of interaction between coordinates.

Experimental	Calculated	σ^2	Var (B)
0.667035	0.667046	1.17E−03	5.58E−05
0.654863	0.654882	6.12E−03	1.08E−05
0.865759	0.865744	1.14E−03	5.21E−03
0.619241	0.619243	5.28E−03	−9.41E−07
0.737095	0.737103	2.10E−03	−4.63E−04
0.677965	0.677949	2.31E−03	−7.17E−05
0.672899	0.672904	4.33E−03	5.32E−06

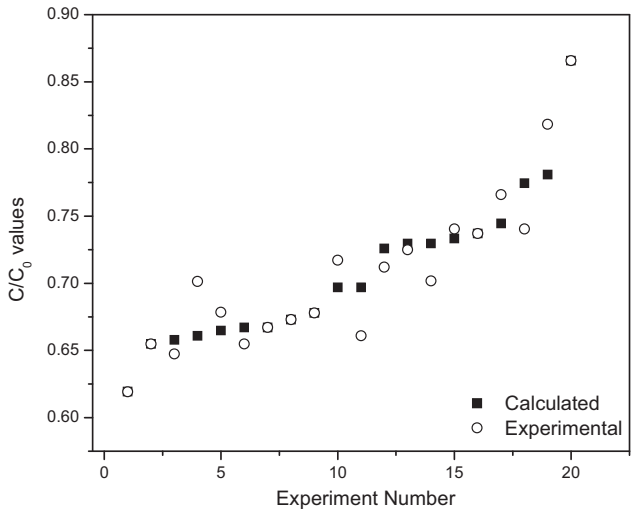

Fig. 6. The plot depicting difference of ratio of final to initial total organic content for experimental and calculated values.

the boundary condition of model applied. The equation was fitted to

$$Y = \left(\frac{2.62}{100}\right)X1 + \left(\frac{1.78}{100}\right)X2 + \left(\frac{6.63}{10}\right)X3 - \left(\frac{6.34}{10000}\right)X1X2 + \left(\frac{2.19}{1000}\right)X1X3 - \left(\frac{2.09}{100}\right)X2X3 + \left(\frac{4.69}{10000}\right)X1X2X3 \quad (16)$$

Table 3
The ratio of final to initial total organic carbon content values of experimental and calculated data with percentage error.

Experimental	Calculated	% Error
0.654841	0.667053	1.864828
0.67856	0.66478	−2.03076
0.701383	0.660991	−5.75888
0.647356	0.657961	1.638207
0.818379	0.78095	−4.57358
0.740439	0.774446	4.592816
0.717251	0.696872	−2.84133
0.660985	0.696872	5.429334
0.76595	0.744571	−2.79118
0.740439	0.733396	−0.95119
0.72498	0.729672	0.647183
0.712042	0.725947	1.952762
0.701709	0.729672	3.984972

where Y = ratio of final to initial organic content, $X1$ = time, $X2$ = sonication energy and $X3$ = applied magnetic field. The equation suggests that the product of time and sonication energy and magnetic field and sonication energy have antagonistic interactions while the product of time and magnetic field factors have synergism with the degradation behaviour. Table 2 summarizes the experimental, calculated and error vectors. Fig. 6 depicts the same in the plot of difference in experimental and calculated values. The coefficient of multiple regression; R^2, is the global statistic to access the fit of a model. In the present study, the value of 0.908 was obtained for the model. Table 3 summarizes the experimental and calculated values of data not included in the model. A maximum of up to 6% variation with the experimental data was observed suggesting the goodness of model.

3.4. Conclusions

The role of bimetallic nanopowder of iron–nickel has been studied for the first time for the degradation of organics in mixed wastes under combined influence of magnetic field and sonicaton energy. The advantage of the bimetallic is in situ generation of hydrogen peroxide that contributes to the degradation of organics. The mixture of organics enhances the rate of degradation. The experimental design model constructed from variables of time, magnetic field and sonication energy constructed from seven experimental data points could predict total organic content data for 13 experimental points not included in the model. It is anticipated that this statistical model can be used as an effective design tool for scaling up a sono-magnetic process for waste treatment using nanoscale iron–nickel.

Acknowledgements

The authors thank Marie Curie Fellowship funded by European Commissions Grants Agreement Number MKTD-CT-2006-042637 and Finnish Cultural Foundation for the financial support for this work. They also thank Ms. Eveliina Repo for ICP-OES analysis, Mr. Vivre for ICP-MS analysis, University of Helsinki for providing XRD facility and Mikkeli University of Applied Sciences for SEM facility.

References

[1] A.P. Toste, R.B. Lucke, T.J. Lechner-Fish, D.J. Hendrren, R.B. Myers, Organic analysis of mixed nuclear waste, Waste Manage. 87 (3) (1987) 323–329.
[2] A.P. Toste, T.J. Lechner-Fish, D.J. Hendren, R.D. Scheele, W.G. Richmond, Analysis of organics in highly radioactive wastes, J. Radioanal. Nucl. Chem. 123 (1) (1998) 149–166.
[3] B.A. Tomkins, J.E. Caton Jr., G.S. Fleming, M.E. Garcia, S.H. Harmon, R.L. Schenley, L.J. Wachte,.H. Griest, Determination of regulatory organic compounds in radioactive waste samples. Volatile organics in aqueous liquids, Anal. Chem. 61 (1989) 2751–2756.

[4] A.P. Toste, T.J. Lechner-Fish, Organic diagenesis in commercial, low level nuclear wastes, Rad. Waste Manage. Nucl. Fuel Cycle 12 (1) (1989) 291–301.
[5] B.A. Tomkins, J.E. Caton Jr., M.D. Edwards, M.E. Garcia, R.L. Schenley, C.A. Trese, W.H. Griest, Determination of regulatory organic compounds in radioactive waste samples. Semivolatile organics in aqueous liquids, Anal. Chem. 62 (1990) 253–257.
[6] A.I. Rybal'chenko, M.K. Pimenov, V.D. Balukova, A.V. Nosukhin, E.I. Mikerin, N.N. Egorov, I.M. Kosareva, V.M. Kurochkin, Glubinnoe zakhoronenie zhidkikh radioaktivnykh otkhodov (Deep-well Disposal of Liquid Radioactive Wastes), IzDat, Moscow, 1994, p. 63.
[7] D.J. Bradlay, C.W. Frank, Y. Mikerin, Nuclear contamination from weapons complexes in the former Soviet Union and the United States, Phys. Today 64 (1996) 40–45.
[8] J.S. Boles, K. Ritchie, D.A. Crerar, Reducing the potential for migration of radioactive waste: aqueous thermal degradation of the chelating agent disodium EDTA, Nucl. Chem. Waste Manage. 7 (1987) 89–93.
[9] R.W.D. Killey, J.O. Mchugh, D.R. Champ, E.L. Cooper, J.L. Young, Subsurface cobalt-60 migration from a low-level waste disposal site, Environ. Sci. Technol. 18 (1984) 148–157.
[10] T.F. Rees, L.M. Cleveland, Environmental Migration of Long-Lived Radionuclides, in: International Atomic Energy Agency, Vienna, Austria, IAEA-SM-257/66~, 1982, p. 41.
[11] R.S. Martin, S.E. Manahan, J. Steven Morris, Fates of radioactive arsenic, cesium, strontium and organo-chlorine during the gasification of mixed wastes in the presence of organic matter, Chemosphere 37 (1998) 531–540.
[12] N. Gokulakrishnan, A. Pandurangan, P.K. Sinha, Catalytic wet peroxide oxidation technique for the removal of decontaminating agents ethylenediaminetetraacetic acid and oxalic acid from aqueous solution using efficient Fenton type Fe-MCM-41 mesoporous materials, Ind. Eng. Chem. Res. 48 (2009) 1556–1561.
[13] W.J. Cooper, R.A. Dougal, M.G. Nickelsen, T.D. Waite, C.N. Kurucz, K.J. Lin, J.P. Bibler, Benzene destruction in aqueous waste 1. Bench-scale gamma-irradiation experiments, Radiat. Phys. Chem. 48 (1996) 81–87.
[14] A.P. Toste, K.J. Polach, T.W. White, Degradation of citric acid in a simulated, mixed nuclear waste: radiolytic versus chemical forces, Waste Manage. 14 (1994) 27–34.
[15] D.F Laine, I.F. Cheng, The destruction of organic pollutants under mild reaction conditions: a review, Microchem. J. 85 (2007) 183–193.
[16] D.W. Tedder, E.P. Horwitz, Concepts in waste management: decontamination of plutonium-bearing mixed wastes with efficient water and acid recycle, Sep. Sci. Sep. Sci. Technol. 38 (2003) 2923–2950.
[17] A.P. Toste, Gamma radiolysis of EDTA in a simulated, mixed nuclear waste, J. Radioanal. Nucl. Chem. 235 (1998) 213–219.
[18] L. Chang, C. Than, H. Morimoto, P.G. Williams, Catalytic oxidation of mixed wastes containing high organic content-emission reduction and the effect of steam, J. Environ. Sci. Health Part A 41 (2006) 47–63.
[19] K.L. Ogden, G.E. Ogden, J.L. Hanners, P.J. Unkefer, Remediation of low-level mixed waste: cellulose-based materials and plutonium, J. Hazard. Mater. 51 (1996) 115–130.
[20] W. Zhang, Nanoscale iron particles for environmental remediation: an overview, J. Nanoparticle Res. 5 (2003) 323–332.
[21] G. Ona, V. Tomas, S. Arvydas, N. Ona, Decontamination of solutions containing EDTA using metallic iron, J. Hazard. Mater. 159 (2008) 446–451.
[22] Y. Lin, C. Weng, F. Chen, Effective removal of AB24 dye by nano/micro-size zero-valent iron, Sep. Purif. Technol. 64 (2008) 26–30.
[23] D.M. Cwiertny, S.J. Bransfield, A.L. Roberts, Influence of the oxidizing species on the reactivity of iron-based bimetallic reductants, Environ. Sci. Technol. 41 (2007) 3734–3740.
[24] X. Li, D.W. Elliott, W. Zhang, Zero-valent iron nanoparticles for abatement of environmental pollutants: materials and engineering aspects, Crit. Rev. Solid State Mater. Sci. 31 (2006) 111–122.
[25] C. Lee, D.L. Sedlak, Enhanced formation of oxidants from bimetallic nickel–iron nanoparticles in the presence of oxygen, Environ. Sci Technol. 42 (22) (2008) 8528–8533.
[26] A.D. Bokare, R.C. Chikate, C.V. Rode, K.M. Paknikar, Effect of surface chemistry of Fe–Ni nanoparticles on mechanistic pathways of azo dye degradation, Environ. Sci Technol. 41 (21) (2007) 7437–7443.
[27] B. Schrick, J.L. Blough, A.D. Jones, T.E. Mallouk, Hydrodechlorination of trichloroethylene to hydrocarbons using bimetallic nickel–iron nanoparticles, Chem. Mater. 14 (2002) 5140–5147.
[28] Y.H. Tee, E. Grulke, D. Bhattacharyya, Role of Ni/Fe nanoparticle composition on the degradation of trichloroethylene from water, Ind. Eng. Chem. Res. 44 (2005) 7062–7070.
[29] L. Gui, R.W. Gillham, M.S. Odziemkowski, Reduction of N-nitrosodimethylamine with granular iron and nickel-enhanced iron. 1. Pathways and kinetics, Environ. Sci. Technol. 34 (2000) 3489–3494.
[30] M.S. Odziemkowski, L. Gui, R.W. Gillham, Reduction of N-nitrosodimethylamine with granular iron and nickel-enhanced iron. 2. Mechanistic studies, Environ. Sci. Technol. 34 (2000) 3495–3500.
[31] L.A. Worl, D. Delvin, D. Hill, Particulate capture of plutonium by HGMS with advanced matrices, Sep. Sci. Technol. 36 (2001) 1335–1349.
[32] R.D. Ambashta, M. Sillanpaa, Water purification using magnetic assistance, a review, J. Hazard. Mater. 180 (2010) 38–49.
[33] Y. Zheng, C. Duanmu, Y. Gao, A magnetic nanocatalyst for cleaving phosphoester and carboxylic ester bonds under mild conditions, Org. Lett. 8 (2006) 3215–3217.
[34] D. Beydoun, R. Amal, J. Scott, G. Low, S. McEvoy, Studies on the mineralization and separation efficiencies of a magnetic photocatalyst, Chem. Eng. Technol. 24 (2001) 745–748.
[35] L. Li, M. Fan, R.C. Brown, L.J. Van, J. Wang, W. Wang, Y. Song, P. Zhang, Synthesis, Properties, and environmental applications of nanoscale iron-based materials: a review, Crit. Rev. Environ. Sci. Technol. 36 (2006) 405–431.
[36] F. Méndez-Arriaga, R.A. Torres-Palma, C. Pétrier, S. Esplugas, J. Gimenezd, C. Pulgarinc, Ultrasonic treatment of water contaminated with ibuprofen, Water Res. 42 (2008) 4243–4248.
[37] V. Naddeoa, S. Meric, D. Kassinos, V. Belgiorno, M. Guida, Fate of pharmaceuticals in contaminated urban wastewater effluent under ultrasonic irradiation, Water Res. 43 (2009) 4019–4027.
[38] H. Ghodbane, O. Hamdaoui, Degradation of Acid Blue 25 in aqueous media using 1700 kHz ultrasonic irradiation: ultrasound/Fe(II) and ultrasound/H_2O_2 combinations, Ultrason. Sonochem. 16 (2009) 593–598.
[39] H. Shemer, N. Narkis, Sonochemical removal of trihalomethanes from aqueous solutions, Ultrason. Sonochem. 12 (2005) 495–499.
[40] J.A. Zazo, J.A. Casas, A.F. Mohedano, M.A. Gilarranz, J.J. Rodriguez, Chemical pathway and kinetics of phenol oxidation by Fenton's reagent, Environ. Sci. Technol. 39 (2005) 9295–9302.
[41] M.J. Watt, K.G. Linden, Advanced oxidation kinetics of aqueous trialkyl phosphate flame retardants and plasticizers, Environ. Sci. Technol. 43 (2009) 2937–2942.
[42] R.A.P. Thomas, L.E. Macaskie, Biodegradation of tributyl phosphate by naturally occurring microbial isolates and coupling to the removal of uranium from aqueous solution, Environ. Sci. Technol. 30 (1996) 2371–2375.
[43] C. Berne, B. Allainmat, D. Garcia, Tributyl phosphate degradation by Rhodopseudomonas palustris and other photosynthetic bacteria, Biotechnol. Lett. 27 (2005) 561–566.
[44] R.A.P. Thomas, K. Lawlor, M. Bailey, L.E. Macskie, Biodegradation of metal-EDTA complexes by an enriched microbial population, Appl. Environ. Biotechnol. 64 (1998) 1319–1322.
[45] T. Zhou, X. Lu, J. Wang, F. Wong, Y. Li, Rapid decolorization and mineralization of simulated textile wastewater, in a heterogeneous Fenton like system with/without external energy, J. Hazard. Mater. 165 (2009) 193–199.
[46] C.R. Keenan, D.L. Sedlak, Ligand-enhanced reactive oxidant generation by nanoparticulate zero-valent iron and oxygen, Environ. Sci. Technol. 42 (2008) 6936–6941.
[47] D.F. Laine, A. Blumenfeld, I.F. Cheng, Mechanistic study of the ZEA organic pollutant degradation system: evidence for H_2O_2, HO, and the homogeneous activation of O_2 by Fe^{II}EDTA, Ind. Eng. Chem. Res. 47 (2008) 6502–6508.
[48] T. Zhou, Y. Li, F. Wong, X. Lu, Enhanced degradation of 2,4-dichlorophenol by ultrasound in a new Fenton like system (Fe/EDTA) at ambient circumstance, Ultrason. Sonochem. 15 (2008) 782–790.
[49] I. Sanchez, F. Stuber, J. Font, A. Fortuny, A. Fabregat, C. Bengo, Elimination of phenol and aromatic compounds by zero valent iron and EDTA at low temperature and atmospheric pressure, Chemosphere 68 (2007) 338–344.
[50] C. Cau Dit Coumesa, S. Courtois, Cementation of a low-level radioactive waste of complex chemistry. Investigation of the combined action of borate, chloride, sulfate and phosphate on cement hydration using response surface methodology, Cement Concrete Res. 33 (2003) 305–316.
[51] M.N. Chong, B. Jina, C.W.K. Chow, C.P. Saint, A new approach to optimise an annular slurry photoreactor system for the degradation of Congo Red: statistical analysis and modeling, Chem. Eng. J. 152 (2009) 158–166.
[52] I. Grcic, M. Muzic, D. Vujevi, N. Koprivanac, Evaluation of atrazine degradation in UV/FeZSM-5/H_2O_2 system using factorial experimental design, Chem. Eng. J. 150 (2009) 476–484.
[53] M.N. Chong, H.Y. Zhuc, B. Jin, Response surface optimization of photocatalytic process for degradation of Congo Red using H-titanate nanofiber catalyst, Chem. Eng. J. 156 (2010) 278–285.
[54] M.A. Islam, V. Sakkas, T.A. Albanis, Application of statistical design of experiment with desirability function for the removal of organophosphorus pesticide from aqueous solution by low-cost material, J. Hazard. Mater. 170 (2009) 230–238.
[55] H. Zhang, H.J. Choi, P. Canazo, C. Huang, Multivariate approach to the Fenton process for the treatment of landfill leachate, J. Hazard. Mater. 161 (2009) 1306–1312.
[56] R. Valenzuela, D. Contreras, C. Oviedo, J. Freer, J. Rodríguez, Copper catechol-driven Fenton reactions and their potential role in wood degradation, Int. Biodeter. Biodegr. 61 (2008) 345–350.
[57] G. Annadurai, L.Y. Ling, J. Lee, Statistical optimization of medium components and growth conditions by response surface methodology to enhance phenol degradation by Pseudomonas putida, J. Hazard. Mater. 151 (2008) 171–178.